ANALYSIS OF TECHNOLOGICAL REGIMES OF OPEN-DIE FORGING WITH MODEL DEVELOPMENT FOR DIGITAL SYSTEMS OF METALLURGICAL PRODUCTION

Volodymyr KUKHAR [1 *], Elena BALALAYEVA [2], Hlib KHLIESTOV [3], Olha KHLIESTOVA [4], Sergiu MAZURU [5]

Contemporary metallurgy requires the efficient production of large-scale components by open-die forging. The paper analyzes the influence of technological parameters (relative bite infeed and relative reduction per pass) on the kinematic (relative elongation) and energy-force (reduced force and reduced work) characteristics of cogging in combined dies. FEM simulations (LS-DYNA) were used for data generation. Based on this data, analytical and high-fidelity AI surrogate models were developed. It is established that both parameters have a monotonic effect on the metrics: narrower infeed maximizes elongation, and reduction determines the absolute load level. The resulting models are intended for embedding in digital twins and automated forging schedule optimization systems.

Keywords: open-die forging, finite element method (FEM), artificial intelligence (AI), modeling, cogging.

1. Introduction

In contemporary metallurgy, a key task is in-house production of critical components – rolling-mill rolls, roller-table rollers, mill spindles, and other heavy-duty parts – manufactured by open-die forging [1, 2]. Elongation forging (cogging) in combined dies – tools with dissimilar upper and lower die geometries – plays a special role, as it enables flexible control of the stress-strain state (SSS) and more effective tailoring of forging geometry and microstructure. Rational selection of process

* Corresponding author
[1] Prof., Dept. of Metallurgy and Production Organization, "Technical University "Metinvest Polytechnic" LLC, Zaporizhzhia, Ukraine, e-mail: kvv.mariupol@gmail.com (corresponding author)
[2] Ass. Prof., Dept. of Information Technologies, Pryazovskyi State Technical University, Dnipro, Ukraine, e-mail: balalaevaeu@gmail.com
[3] PhD student, Dept. of Metallurgy and Processing of Metals, Pryazovskyi State Technical University, Dnipro, Ukraine, e-mail: glebkhlestov@gmail.com
◊ This paper is drawn up to be presented, as appropriate, in a section of ICAMaT 2025
[4] Head of the Dept. of Heat Power Engineering and Environmental Protection, Pryazovskyi State Technical University, Dnipro, Ukraine, e-mail: hlestova182@gmail.com
[5] Head of the Dept. of Manufacturing Engineering, Technical University of Moldova, Chisinau, Moldova, e-mail: sergiu.mazuru@tcm.utm.md

parameters – feed (bite infeed), reduction per pass, and die geometry – is essential to boost productivity, reduce energy consumption, and ensure product quality [1, 2].

In industrial practice, shop forging schedules are often experience-driven rather than analytics-based, which does not always provide an optimal energy–quality balance. Consequently, studies employing experiments, the finite element method (FEM), and mathematical model building are increasingly important for the formal selection of cogging regimes [2, 3].

The objective of this work is to analyze the influence of tool geometry (bite width/feed) and reduction magnitude on kinematic and energy–force characteristics of forging in combined dies. LS-DYNA simulations derive analytical relationships between process parameters and deformation outcomes to support AI training and automated optimization of open-die forging schedules.

We first consider studies focusing on austenite stability and microstructural mechanisms, as these define the boundary conditions for selecting die geometry and reduction. Metastable austenite can transform to martensite under load, altering local stiffness and friction; these effects must be reflected in analytical models [4]. Constitutive approaches describe the interplay of recrystallization, hardening, and phase transformations ($Q \approx 374$ [kJ/mol], where Q denotes the apparent activation energy) [5], while microstructural anisotropy and the deformation path govern fatigue crack resistance, calling for control of grain shape/texture [6]. Experimental–FEM studies on large ingots further show that the deformation route, particularly die geometry, dictates strain inhomogeneity and microstructure [7].

We next examine the influence of die geometry and contact. Upsetting with conical ledges concentrates compression in the core and promotes defect closure [8]; narrow-die indentation provides controllable widening, contact length, and diameter change for targeted elongation at lower peak loads [9]. Pre-upsetting with convex dies and load eccentricity reduces internal stresses and scrap through pre-profiling of metal flow [10]. Comparative studies show that convex dies intensify elongation, concave dies create predominantly compressive fields with lower cracking risk, whereas flat dies tend to induce tension and critical stresses [11]. FEM-designed V-die tests combined with optimized friction testing enable rapid workability assessment and parameter selection for low-ductility alloys [12]. Two-stage forging ($\varepsilon_{h\%} \approx 5$ [%] + $\varepsilon_{h\%} \approx 15$ [%], where $\varepsilon_{h\%}$ – the relative reduction per stage) refines the structure and improves roll life [2]. Hybrid dies (X38CrMoV5.3 + Inconel 718) reveal the strong effect of tool material combinations on press force and flow [13]. Miniaturized rigs reproduce recrystallization over 20–600 [°C], enabling rapid screening of feed/reduction schedules [14]. A Billet Quality Index with FEM+Taguchi+DNN (deep neural network) shortens process time and improves quality [1]. Industrial cogging of a 3.3-tonne ingot confirms the importance of pass scheduling and the adequacy of FEM predictions [15]. Void-closure models for AISI 410 steel agree with experiments within ~7 [%], supporting die geometry and

feed/reduction selection [16]. Finally, steel properties depend on pass parameters, per-pass reduction, and die from [17], while friction conditions govern barreling (strain inhomogeneity) and thus the effective contact length and press load [18].

Next, we address energy efficiency. A rational combination of upsetting and cogging ($h/D_0 \approx 2$, where h [mm] is the billet height and D_0 [mm] is the billet diameter) reduces strain nonuniformity and energy use by 20–30 [%] [19]. Data-driven methods that incorporate friction uncertainty provide sufficient accuracy for rapid on-line tuning [20]. Generalized predictive control (GPC) stabilizes the energy–force parameters [21], while fast models integrated with thermography enable on-the-fly correction of the pass schedule [22]. In parallel, a geometry-feature-based cost estimation method supports early-stage route and press selection [23].

A separate stream involves AI and surrogate models. Neural networks achieve FEM-like accuracy in stress–strain prediction [24]. CrystalMind accelerates computation by 36× with <2 [%] recrystallization error [25]. Double Deep Q-Learning optimizes forging pass schedules [26], and DeepForge combines AI with model-predictive control for microstructural regulation [27]. Manipulator-based strategies enable intentional curvature of parts [28], while fusing 3D metrology with FEM databases improves pass selection [29].

Finally, sensor technologies. Automated temperature-field control maintains plasticity and supports energy-consumption models [30]. High-precision 3D metrology of heavy forgings improves elongation assessment reliability [31]. Concepts fusing geometry and temperature measurements enable real-time adaptation of forging regimes [32, 33].

In view of the above analysis, combining FEM for primary data acquisition with AI methods for data processing can provide the basis for mathematical models designed to enable control and optimization of open-die forging regimes.

2. Materials and methods

A concise thematic aggregation and critical screening of sources were used to define the control variables – relative bite infeed B/D_0 (where B [mm] is the bite length) and the relative reduction $\varepsilon_{h\%} = \Delta h/D_0$ (where Δh [mm] is the height reduction per pass) – as well as the normalized outputs (relative elongation δ [%]; reduced forging force f [N/mm] – force F [N] per unit die width B [mm]; and reduced deformation work w [J/mm] – deformation work W [J] per unit die width B [mm]) which were subsequently defined and evaluated within the modelling framework.

Geometry, Materials, and Finite-element setup. Geometry and initial dimensions were defined as follows. The billet (ingot model) was a cylinder with $D_0 = 550$ [mm] and initial length $L_0 = 1300$ [mm], made of 25Kh1M1F / 25Cr1Mo1V steel (nominal wt.[%]: C = 0.23–0.29, Si = 0.20–0.40, Mn = 0.40–

0.70, Cr = 0.90–1.20, Mo = 0.90–1.20, V = 0.20–0.30, P ≤ 0.030, S ≤ 0.025; Fe – balance). The combined dies comprised a flat upper die and a grooved lower die with a 300 [mm] fillet radius (Fig. 1a). Hot deformation was simulated in LS-DYNA at ~1100 [°C] (isothermal) with an upper-die speed of 50 [mm/s].

The numerical simulation followed a standard staged finite-element workflow, including geometry definition, mesh generation, material model assignment, specification of boundary and contact conditions, numerical solution, and post-processing. The billet and dies were defined directly using analytical geometry without importing external CAD models; the dies were treated as rigid bodies, and Coulomb-type friction was applied. Boundary conditions included prescribed upper-die displacement and a constrained lower die.

The billet was discretized using a three-dimensional tetrahedral finite-element mesh with a characteristic element size of ~10 [mm], selected as a compromise between numerical accuracy and computational efficiency for large-scale open-die forging simulations. This resolution is sufficient to capture strain and stress gradients governing elongation, force, and deformation work during single-bite reduction, and was previously validated for energy-force and kinematic parameters; the corresponding finite-element solid-state model with discretization mesh is shown in Fig. 1b.

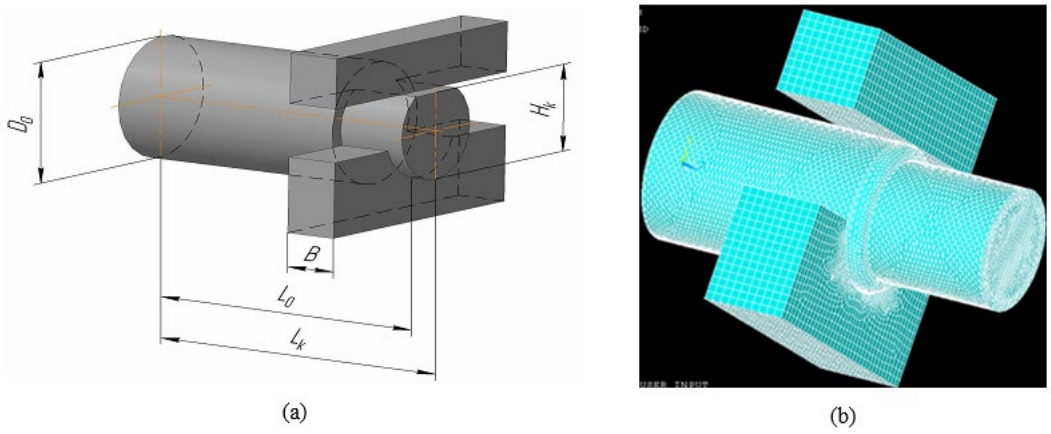

Fig. 1. Schematic of billet reduction during cogging in combined dies (a) and finite-element solid-state model with discretization mesh (b):
D_0, L_0 and L_k – initial diameter, initial and final length of the workpiece during cogging;
H_k – final height of the workpiece after crimping; B – die (bite) width

Load Focus and Regime Coding. To represent peak energy–force demand typical of industrial cogging routes, analysis focused on the first reduction immediately after each feed, where the contact area is maximal. This rationale covers (i) alternating feeds of fixed magnitude with circumferential “re-bites”

(radial compressions) at each feed position and (ii) routes with fixed reduction on sequential feeds along the billet followed by rotations and repeats toward the target diameter – under otherwise equal conditions, the first pass governs the peak load. To limit scope without losing relevance, only single-bite compressions of identically sized billets were simulated per setting; regimes were labeled by a compact code "reduction [mm]*bite width [mm]" (e.g., 66*240).

Design of computational experiments. The computational experiment followed a full-factorial 3×3 design: bite widths B = 180 / 240 / 300 [mm] (B/D_0 = 0.327 / 0.436 / 0.545) crossed with reductions per pass Δh = 50 / 66 / 100 [mm] ($\varepsilon_{h\%}$ = 9.09 / 12.0 / 18.18 [%]). For each combination, a single reduction was computed and the normalized outputs recorded. The global forging ratio is defined as $k = (D_0/D_f)^2$ for the final diameter D_f. From the simulated data, response surfaces and working plots of the mappings "feed/reduction → elongation/force/work" were constructed as the basis for model identification.

Normalized (reduced) metrics were defined as follows:

$$\delta = 100 \times (\Delta L/L_0), \tag{1}$$

where $\Delta L = (L_f - L_0)$ is the absolute elongation [mm], with initial L_0 [mm] and final L_f [mm]billet lengths after the simulated reduction.

$$f = F/B, \tag{2}$$

$$w = W/B\,, \tag{3}$$

Normalizing F and W by B removes the trivial scale effect of bite width and makes energy–force comparisons across regimes physically meaningful.

Data post-processing and model identification. Regression identification was applied to the simulated datasets: linear models with interaction terms; power-law and exponential transforms; compact cubic polynomials (engineering form) and a high-fidelity quartic surrogate; as well as a hybrid nonlinear "power×exponential" form estimated by least squares and Levenberg–Marquardt. Model selection relied on coefficient of determination (R^2), root mean squared error (RMSE), Akaike Information Criterion (AIC) / Bayesian/Schwarz Information Criterion (BIC), residual diagnostics, and physics-based plausibility checks (monotonicity with reduction; non-negativity of force/work). Standard AI tooling (automated parameter search and basic cross-validation) assisted screening, but the final governing relations were established via classical regression. The selected control-oriented surrogates are intended for embedding into digital twins and decision-support/model-predictive control to enable subsequent automation of open-die forging optimization.

3. Results and discussions

The FEM simulations in combined dies quantify how the relative bite B/D_0 and the per-pass reduction $\varepsilon_{h\%}$ affect elongation as well as the force and deformation work. In cogging routes with alternating feeds of fixed magnitude and circumferential "re-bites" (radial compressions) at each feed position, the maximum die–workpiece contact area occurs at the first reduction after a feed, as also reported in [4]. Consequently, the peak energy–force demand of cogging corresponds to this first reduction, and on the first pass respectively.

This rationale allowed us to limit the study to single-bite compressions of billets with identical initial dimensions while varying feed and reduction. As a result, the elongation, force, and deformation work versus die width were obtained (Table 1); all values were converted to normalized, width-reduced metrics (see Table 1).

Table 1

Results of single-bite cogging simulations for different reduction–bite combinations

Forging mode code (reduction [mm]*bite [mm])	ΔL [mm]	δ [%]	F [MN]	f [kN/mm]	W [kJ]	w [J/mm]
50*300	15.1	5.0	1.86	6.2	36.2	121
50*240	13.8	5.8	1.62	6.8	32.4	135
50*180	12.5	6.9	1.46	8.1	29	161
66*300	23.51	7.8	2.12	7.1	55.2	184
66*240	22.3	9.3	1.91	8.0	49.8	208
66*180	19.6	10.9	1.7	9.4	44.2	246
100*300	47.5	15.8	2.76	9.2	103	343
100*240	43.3	18.0	2.42	10.1	92.6	386
100*180	38.7	21.5	2.12	11.8	82.6	459

The dependences of relative elongation, reduced force, and reduced deformation work on the relative die width at different reductions are presented in Figs. 2–4. Across all reductions ($\varepsilon_{h\%}$ = 9.09, 12, and 18.18 [%]), increasing the relative bite B/D_0 leads to a monotonic decrease in all three metrics, indicating that wider bites reduce elongation, force, and deformation work per pass.

For relative elongation (Fig. 2), the curves scale chiefly with $\varepsilon_{h\%}$: the highest reduction (18.18 [%]) yields the largest δ (~21 [%] → 16 [%]), followed by 12 [%] (~11 [%] → 8 [%]) and 9.09 [%] (~6.9 [%] → 5 [%]), showing that δ is more sensitive to reduction than to bite within the tested range.

As shown in Fig. 3, the reduced forging force f [N/mm] decreases with increasing B/D_0, with its absolute level governed primarily by the reduction $\varepsilon_{h\%}$ such that f(18.18 [%]) > f(12 [%]) > f(9.09 [%]) at any given B/D_0. A similar trend is observed for the reduced deformation work w (Fig. 4), for which w(18.18 [%]) > w(12 [%]) > w(9.09 [%]) across the entire B/D_0 range. Over B/D_0 = 0.33–0.55, both f and w decrease by approximately 15–25 [%], indicating

that wider bites lower the energy-force demand per unit bite width, with the strongest sensitivity at $\varepsilon_{h\%} = 18.18$ [%].

After processing the graphical dependences in Fig. 2–4, analytical relationships were obtained to calculate the energy–force and kinematic parameters of the most energy-intensive open-die forging modes on the investigated dies with high reliability (coefficient of determination $R^2 \geq 0.98$).

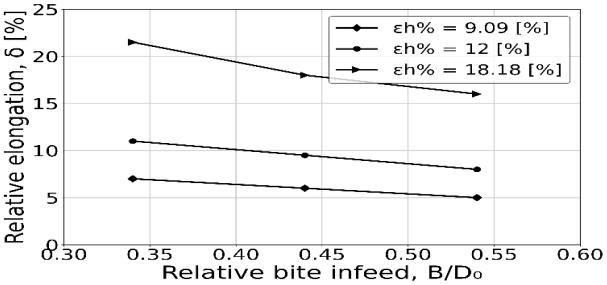

Fig. 2. Relative billet elongation (δ) versus relative bite infeed (B/D_0) at different reductions ($\varepsilon_{h\%}$) in combined dies

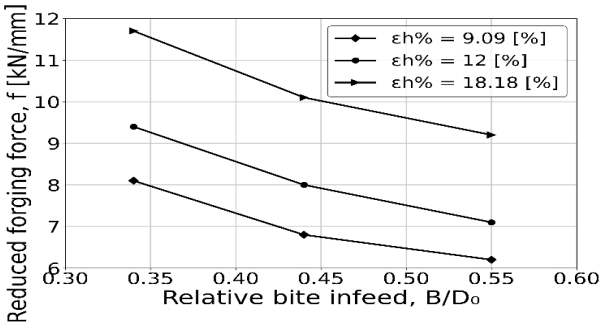

Fig. 3. Reduced forging force (f) versus relative bite infeed (B/D_0) at different reductions ($\varepsilon_{h\%}$) in combined dies

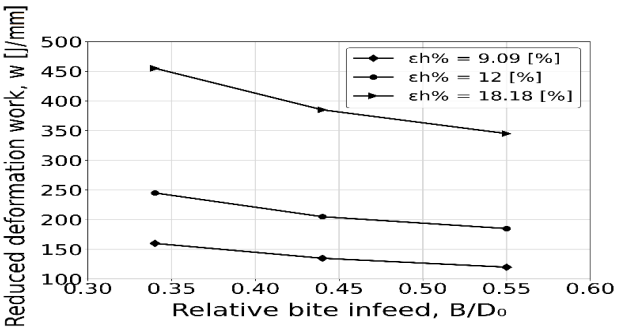

Fig. 4. Reduced deformation work (w) versus relative bite infeed (B/D_0) at different reductions ($\varepsilon_{h\%}$) in combined dies

The analytical relationships (4)–(6), which reflect the influence of forging parameters on relative elongation $\delta_{FEM}(B/D_0, \varepsilon_{h\%})$, reduced force $f_{FEM}(B/D_0, \varepsilon_{h\%})$ and reduced deformation work $w_{FEM}(B/D_0, \varepsilon_{h\%})$ were obtained as a result of numerical simulation by the finite element method (FEM):

$$\delta_{FEM} = (-1.92 \cdot \varepsilon_{h\%} + 8.766) \cdot (B/D_0) + 2.23 \cdot \varepsilon_{h\%} - \\ -10.84;\ (R^2 = 0.996); \quad (4)$$

$$f_{FEM} = a_f \cdot (B/D_0)^2 + b_f \cdot (B/D_0) + c_f;\ \ (R^2 \approx 1), \quad (5)$$

where $a_f = 0.5429 \cdot \varepsilon_{h\%}^2 - 14.343 \cdot \varepsilon_{h\%} + 114.98$; $b_f = -0.4286 \cdot \varepsilon_{h\%}^2 + \\ +10.931 \cdot \varepsilon_{h\%} - 98.35$; $c_f = 0.0757 \cdot \varepsilon_{h\%}^2 - 1.4583 \cdot \varepsilon_{h\%} + 23.204$;

$$w_{FEM} = \mathrm{a_w} \cdot (\mathrm{B/D_0})^2 + \mathrm{b_w} \cdot (\mathrm{B/D_0}) + \mathrm{c_w};\ \ (R^2 \approx 1), \quad (6)$$

where $a_w = 8.8039 \cdot \varepsilon_{h\%}^2 - 156.75 \cdot \varepsilon_{h\%} + 1202.4$; $b_w = -8.2708 \cdot \varepsilon_{h\%}^2 + \\ +114.53 \cdot \varepsilon_{h\%} - 981.51$; $c_w = 2.3417 \cdot \varepsilon_{h\%}^2 - 3.6815 \cdot \varepsilon_{h\%} + 150.98$.

The analytical relationships (7)–(15) were obtained using artificial intelligence (AI). In this study, AI was applied as an auxiliary analytical tool within a researcher-controlled workflow. Specifically, a large language model (ChatGPT, version 5.2) was used to assist in the formulation, structuring, and symbolic handling of regression models, while all model forms and assumptions were explicitly defined and validated by the researchers. The final regression equations were implemented and evaluated using standard numerical procedures, including ordinary least squares and nonlinear regression. Based on the experimental dataset, approximation dependencies $\delta_i(B/D_0, \varepsilon_{h\%})$, $f_i(B/D_0, \varepsilon_{h\%})$, $w_i(B/D_0, \varepsilon_{h\%})$ were constructed. Different model classes were considered: additive linear – (7), (10), (13); linear with interaction – (8); second-order polynomial – (9), (12), (14); and multiplicative power-law models – (11), (15).

$$\delta_1 = -16.667 \cdot (B/D_0) + 1.408 \cdot \varepsilon_{h\%} + 0.298;\ \ (R^2 = 0.982); \quad (7)$$

$$\delta_2 = 9.938 \cdot (B/D_0) + 2.302 \cdot \varepsilon_{h\%} - 2.0329.938 \cdot (B/D_0) \cdot \varepsilon_{h\%} - \\ -11.408;\ (R^2 = 0.994); \quad (8)$$

$$\delta_3 = 9.938(\mathrm{B/D_0}) + 1.446\varepsilon_{h\%} - 2.032(\mathrm{B/D_0})\varepsilon_{h\%} + 0.031(\mathrm{B/D_0})^2 - \\ -5.94;\ (R^2 = 0.999); \quad (9)$$

$$f_1 = -10.3 \cdot (B/D_0) + 0.365 \cdot \varepsilon_{h\%} + 8.28;\ (R^2 = 0.999); \quad (10)$$

$$f_2 = 1.28 \cdot (B/D_0)^{-0.522} \cdot (\varepsilon_{h\%})^{0.562};\ (R^2 \approx 1); \tag{11}$$

$$f_3 = 30.23 \cdot (B/D_0) + 0.612 \cdot \varepsilon_{h\%} - 0.330 \cdot (B/D_0) \cdot \varepsilon_{h\%} + 27.55 \cdot (B/D_0)^2 + \\ -0.0036 \cdot \varepsilon_{h\%}^2 + 10.84;\ (R^2 \approx 1); \tag{12}$$

$$w_1 = -330.30 \cdot (B/D_0) + 28.49 \cdot \varepsilon_{h\%} + 21.61;\ (R^2 = 0.997); \tag{13}$$

$$w_2 = -508.11 \cdot (B/D_0) + 32.06 \cdot \varepsilon_{h\%} - 38.27 \cdot (B/D_0) \cdot \varepsilon_{h\%} + \\ +771.35 \cdot (B/D_0)^2 + 0.479 \cdot \varepsilon_{h\%}^2 + 29.11;\ (R^2 \approx 1); \tag{14}$$

$$w_3 = 3.07 \cdot (B/D_0)^{-0.568} \cdot (\varepsilon_{h\%})^{1.509};\ (R^2 \approx 1). \tag{15}$$

Graphs illustrating the dependence of δ, f_i, w on B/D_0 at different degrees of compression $\varepsilon_{h\%}$ were constructed using AI (Fig. 5–7).

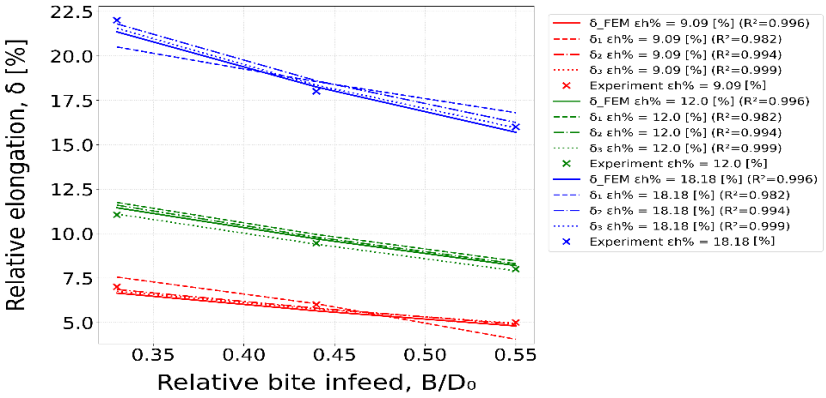

Fig. 5. Relative billet elongation (δ) versus relative bite infeed (B/D_0) at different reductions ($\varepsilon_{h\%}$) in combined dies, obtained using FEM and AI

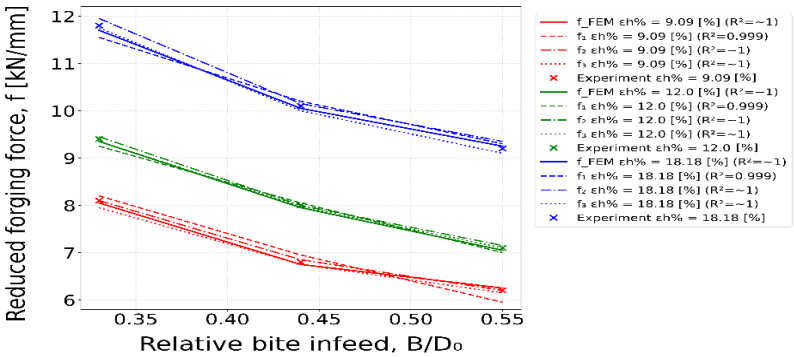

Fig. 6. Reduced forging force (f) versus relative bite infeed (B/D_0) at different reductions ($\varepsilon_{h\%}$) in combined dies, obtained using FEM and AI

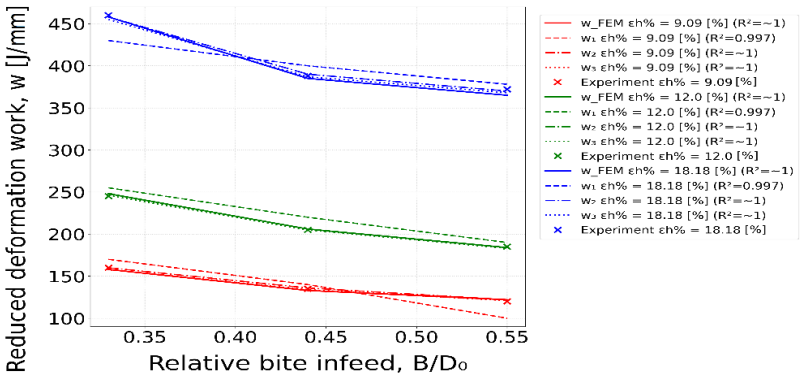

Fig. 7. Reduced deformation work (w) versus relative bite infeed (B/D_0) at different reductions ($\varepsilon_{h\%}$) in combined dies, obtained using FEM and AI

Also, AI automatically determined the optimal coefficients for each model and evaluated their accuracy using the coefficient of determination ($R^2 \geq 0.98$), which demonstrates a high degree of correspondence between the calculated and experimental data for all models. Overall, the second-order polynomial model demonstrates the best results.

3D graphs of the dependences $\delta(B/D_0, \varepsilon_{h\%})$, $f(B/D_0, \varepsilon_{h\%})$, $w(B/D_0, \varepsilon_{h\%})$ for FEM models and AI 2nd order polynomial models were constructed (Fig. 8–10).

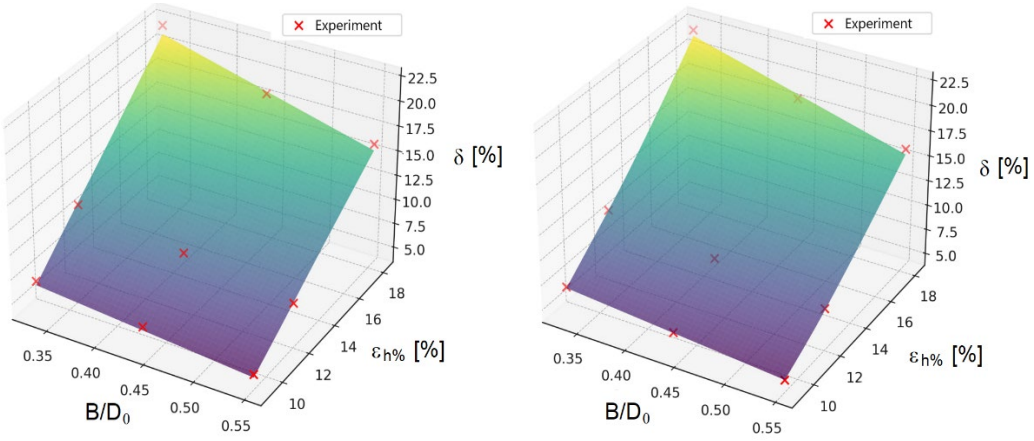

(a) (b)

Fig. 8. Three-dimensional graphs of the dependences $\delta(B/D_0, \varepsilon_{h\%})$ for FEM model (a) and AI 2nd order polynomial model (b)

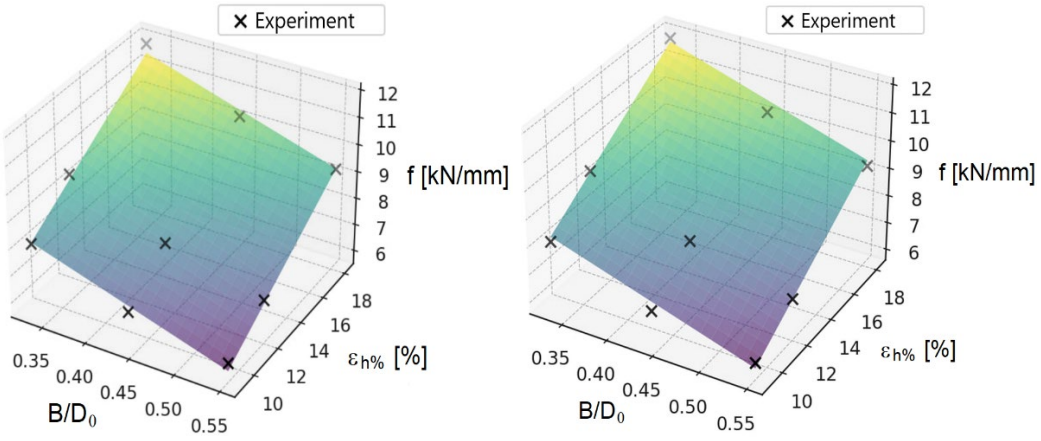

(a) (b)

Fig. 9. Three-dimensional graphs of the dependences $f(B/D_0, \varepsilon_{h\%})$ for FEM model (a) and AI 2nd order polynomial model (b)

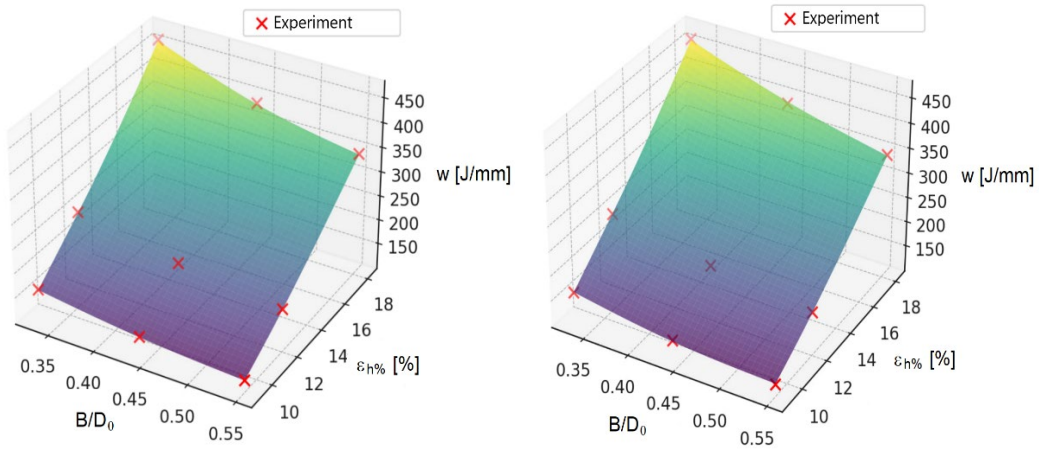

(a) (b)

Fig. 10. Three-dimensional graphs of the dependences $w(B/D_0, \varepsilon_{h\%})$ for FEM model (a) and AI 2nd order polynomial model (b)

In further development, the proposed analytical models are integrated into digital twins (DT) as reduced-order surrogates operating alongside FEM-based offline simulations. FEM results are used to periodically update and recalibrate the regression coefficients, while the surrogate models provide fast online predictions of force, deformation work, and elongation, enabling iterative refinement of forging schedules with respect to energy consumption and process constraints.

4. Conclusions

1. For all investigated reductions, increasing the relative bite infeed B/D_0 causes a monotonic decrease in the normalized metrics (relative elongation δ, reduced forging force f, and deformation work w). This confirms an inherent trade-off of combined-die cogging: narrower bites intensify elongation per pass, whereas wider bites reduce the width-normalized energy-force demand.

2. The reduction magnitude $\varepsilon_{h\%}$ is the dominant factor setting the absolute level of elongation δ, reduced force f, and reduced work w; within the studied range, δ exhibits higher sensitivity to $\varepsilon_{h\%}$ than to B/D_0. The maximum reduction 18.18 [%] consistently yields the highest elongation and the highest normalized force f and deformation work w.

3. The study explicitly targets the most energy-intensive stage of industrial cogging – the first reduction immediately after each feed – because it corresponds to the maximum die-workpiece contact area and governs peak force and deformation work in practical pass schedules.

4. A consistent set of response surfaces $\delta(B/D_0, \varepsilon_{h\%})$, $f(B/D_0, \varepsilon_{h\%})$, $w(B/D_0, \varepsilon_{h\%})$ were identified from the FEM dataset using classical regression and AI-assisted formulation within a researcher-controlled workflow. The obtained relations provide high-fidelity approximation ($R^2 \geq 0.98$), with the quadratic polynomial giving the best overall balance of accuracy and compactness.

5. The developed reduced-order models are suitable for deployment in digital-twin and decision-support loops as fast online surrogates, while FEM remains the offline reference for periodic coefficient recalibration. This enables constrained optimization of forging schedules with respect to energy consumption and process limits without repeated full-scale FEM runs.

REFERENCES

[1] *J. Park, Y. Kim, H. Jeong, H. Kwon, Y. Kwon, N. Kim,* Cogging process design of M50 bearing steel for billet quality, Journal of Materials Research and Technology, Vol. **26**, 2023, DOI: 10.1016/j.jmrt.2023.08.275.

[2] *V. Kukhar, O. Vasylevskyi, K. Malii, V. Zurnadzhy, B. Efremenko, I. Sili,* Development of manufacturing process for high-chromium steel large welding roll, Defect and Diffusion Forum, Vol. **430**, 2024, DOI: 10.4028/p-S55ows.

[3] *D. Connolly, G. Sivaswamy, S. Rahimi, V. Vorontsov,* Miniaturised experimental simulation of open-die forging, Journal of Materials Research and Technology, Vol. **26**, 2023, DOI: 10.1016/j.jmrt.2023.08.073.

[4] *V.I. Zurnadzhy, V.G. Efremenko, M.N. Brykov, I. Petryshynets, T.V. Pastukhova, R.A. Kussa*, The metastability of retained austenite in multiphase steel during abrasive wear, Journal of Friction and Wear, Vol. **41**, Iss. 2, 2020, DOI: 10.3103/S1068366620020178.

[5] *M. Khan, D. Shahriari, M. Jahazi, J.-B. Morin,* Interactions between dynamic softening and strengthening mechanisms during hot forging of a high-strength steel, Frontiers in Mechanical Engineering, Vol. **7**, 2021, DOI: 10.3389/fmech.2021.697116.

[6] *T. Strohmann, E. Breitbarth, M. Besel, S. Zaunschirm, T. Witulski, G. Requena,* Damage mechanisms and anisotropy of an AA7010-T7452 open-die forged alloy: Fatigue crack propagation. Materials, Vol. **15**, Iss. 11, 2022, DOI: 10.3390/ma15113771.

[7] *P. Dhondapure, N. Rajakrishnan, S. Nayak, H. Champliaud, J.-B. Morin, M. Jahazi,* Influence of deformation path on microstructure evolution during the open die forging of large size ingot of high strength steel: Experiments and FE analysis, International Journal of Advanced Manufacturing Technology, Vol. **134**, Iss. 7–8, 2024, DOI: 10.1007/s00170-024-14360-7.

[8] *O.E. Markov, A.S. Khvashchynskyi, A.V. Musorin, M.A. Markova, A.A. Shapoval, N.S. Hrudkina*, Investigation of new method of large ingots forging based on upsetting of workpieces with ledges. International Journal of Advanced Manufacturing Technology, Vol. **122**, Iss. 3–4, 2022, DOI: 10.1007/s00170-022-09989-1.

[9] *V. Chukhlib, E. Klemeshov, S. Gubskyi, A. Okun, N. Biba*, Theoretical and experimental studies of changes in the workpiece shape during narrow die indentation, Lecture Notes in Mechanical Engineering, Springer, 2020, DOI: 10.1007/978-3-030-50794-7_35.

[10] *V. Kukhar, E. Balalayeva, S. Hurkovska, Y. Sahirov, O. Markov, A. Prysiazhnyi, O. Anishchenko*, The selection of options for closed-die forging of complex parts using computer simulation by the criteria of material savings and minimum forging force. Advances in Intelligent Systems and Computing, Springer, Vol. **989**, 2020, DOI: 10.1007/978-981-13-8618-3_35.

[11] *D.I. Buteler, P.C.U. Neves, L.V. Ramos, C.E.R. Santos, R.M. Souza, A. Sinatora,* Effect of anvil geometry on the stretching of cylinders, Journal of Materials Processing Technology, Vol. **179**, Iss. 1–3, 2006, DOI: 10.1016/j.jmatprotec.2006.03.079.

[12] *J. Kotous, V. Kubec, M. Duchek, T. Studecký*, Optimization of workability technological testing for open-die forging, IOP Conference Series: Materials Science and Engineering, Vol. **23**, Iss. 1, 2020, DOI: 10.1088/1757-899X/723/1/012015.

[13] *J. Siring, C. Heine, M. Till, H. Wester, J. Uhe, B.-A. Behrens, K. Brunotte,* Numerical process design for the production of a hybrid die made of tool steel X38CrMoV5.3 and Inconel 718, Materials Research Proceedings, Vol. **41**, 2024, DOI: 10.21741/9781644903131-89

[14] *D. Connolly, G. Sivaswamy, S. Rahimi, V. Vorontsov*, Miniaturised experimental simulation of open-die forging, Journal of Materials Research and Technology, Vol. **26**, 2023, DOI: 10.1016/j.jmrt.2023.08.073.

[15] *K. van Putten, G. Winning*, Best practice analysis of an industrial cogging process for a tool steel ingot, Metallurgia Italiana, Vol. **115**, Iss. 7–8, 2024.

[16] *A. Geisler, M. Sadeghifar, J.-B. Morin, A. Loucif, M. Jahazi*, Void closure during open die forging of large size martensitic stainless-steel ingots: An experimental–analytical–numerical study, International Journal of Material Forming, Vol. **16**, Iss. 1, 2023, DOI: 10.1007/s12289-022-01735-y.

[17] *L. Kander, M. Greger,* Effect of forging ratio on microstructure and grain size of the structural steel used for special applications, METAL 2019 – 28th International Conference on Metallurgy and Materials, TANGER Ltd, 2019.

[18] *V.V. Kukhar, E.S. Klimov, S.M. Chernenko, E.Yu. Balalayeva*, Correlation of barreling effect with boundary friction coefficient during upsetting of various materials workpieces under processing conditions, Materials Science Forum, Vol. **992**, 2020, DOI: 10.4028/www.scientific.net/MSF.992.751.

[19] *K.D. Kolisnyk, V.L. Chukhlib,* Enhancing the energy efficiency of the combined forging operations of upsetting and drawing out, Problems of the Regional Energetics, Vol. **2**, Iss. 66, 2025, DOI: 10.52254/1857-0070.2025.2-66-13.

[20] *K. Chatterjee, U.S. Dixit, J. Zhang, P.A. Petrov*, A methodology for data-driven estimation of forging load, Lecture Notes in Mechanical Engineering, Springer, 2022 DOI: 10.1007/978-981-16-7787-8_2.

[21] *R. Dindorf, J. Takosoglu, P. Wos,* Prediction of the parameters and the hot open die elongation forging process on an 80 MN hydraulic press, Open Engineering, Vol. **11**, Iss. 1, 2021, DOI: 10.1515/eng-2021-0056.

[22] *F. Rudolph, M. Wolfgarten, V. Keray, G. Hirt,* Optimization of open-die forging using fast models for strain, temperature, and grain size in the context of an assistance system, Minerals, Metals and Materials Series, Springer, 2021, DOI: 10.1007/978-3-030-75381-8_96.

[23] *F. Campi, C. Favi, M.Mandolini, M. Germani,* Using design geometrical features to develop an analytical cost estimation method for axisymmetric components in open-die forging, Procedia CIRP, Vol. **84**, 2019, DOI: 10.1016/j.procir.2019.04.324.

[24] *N.V. Jagtap, N. Reinisch, R. Abdusalamov, D. Bailly, M. Itskov*, Modeling of equivalent strain in 2D cross-sections of open die forged components using neural networks, Advances in Industrial and Manufacturing Engineering, Vol. **9**, 2024, DOI: 10.1016/j.aime.2024.100152.

[25] *J. Petrik, S.I. Ali, M. Feistle, M. Bambach*, CrystalMind: A surrogate model for predicting 3D models with recrystallization in open-die hot forging including an optimization framework, Mechanics of Materials, Vol. **189**, 2024, DOI: 10.1016/j.mechmat.2023.104875.

[26] *N. Reinisch, F. Rudolph, S. Günther, D. Bailly, G. Hirt*, Successful pass schedule design in open-die forging using double deep Q-learning. Processes, Vol. **9**, Iss. 7, 2021, DOI: 10.3390/pr9071084.

[27] *J. Petrik, M. Bambach*, DeepForge: Leveraging AI for microstructural control in metal forming via model predictive control. Journal of Manufacturing Processes, Vol. **121**, 2021, DOI: 10.1016/j.jmapro.2024.05.023.

[28] *M. Wolfgarten, F. Rudolph, G. Hirt*, Analysis of process forces and geometrical correlations for open-die forging with superimposed manipulator displacements, Journal of Materials Processing Technology, Vol. **276**, 2020, DOI: 10.1016/j.jmatprotec.2019.116408.

[29] *L. Quentin, R. Beermann, K. Brunotte, B.-A. Behrens, M. Kästner, E. Reithmeier*, Concept of a control system based on 3D geometry measurement for open die forging of large-scale components, In P. J. de Groot, R. K. Leach, & P. Picart (Eds.), Optics and Photonics for Advanced Dimensional Metrology 2020, SPIE, Vol. **11352**, 2020, DOI: 10.1117/12.2554720.

[30] *O. Khrebtova, O. Shapoval, O. Markov, V. Kukhar, N. Hrudkina, M. Rudych*, Control systems for the temperature field during drawing, taking into account the dynamic modes of the technological installation, 2022 IEEE 4th International Conference on Modern Electrical and Energy System (MEES 2022), IEEE, 2022, DOI: 10.1109/MEES58014.2022.10005724.

[31] *J. Hurník, A. Zatočilová, T. Konečná, P. Štarha, D. Koutný*, Multi-view camera system for measurement of heavy forgings, International Journal of Advanced Manufacturing Technology, Vol. **121**, Iss. 11–12, 2022, DOI: 10.1007/s00170-022-09809-6.

[32] *L. Quentin, R. Beermann, K. Brunotte, B.-A.Behrens, M. Kästner, E. Reithmeier*, Concept of a control system based on 3D geometry measurement for open die forging of large-scale components, SPIE, Vol. **11352**, 2020, DOI: 10.1117/12.2554720.

[33] *G. Škulj, D. Bračun*, Geometry and temperature data fusion for automated measurement during open die forging of large hot workpieces, Procedia CIRP, Vol. **93**, 2020, DOI: 10.1016/j.procir.2020.04.127.